Ecological Indicators 150 (2023) 110187

Contents lists available at ScienceDirect

Ecological Indicators

journal homepage: www.elsevier.com/locate/ecolind

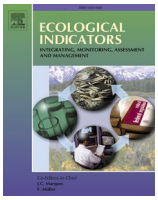

Evaluation of monthly-scale soil erosion spatio-temporal dynamics and identification of their driving factors in Northeast China

Yunfei Cao, Li Hua *, Qi Tang, Lin Liu, Chongfa Cai

College of Resources and Environment, Huazhong Agricultural University, Wuhan 430070, China

ARTICLE INFO

Keywords:
Monthly soil erosion
RUSLE
Geographic Information Science
The logarithmic mean Divisia index
Random Forest

ABSTRACT

Soil water erosion has caused an enormous damage to agricultural production and ecosystems worldwide. Soil erosion exhibits certain seasonal variation patterns within year under the influence of multiple factors. In this study, we calculated the multi-year average monthly-scale soil erosion modulus from 2001 to 2019 to evaluate the soil erosion risk using the revised universal soil loss equation (RUSLE) in the black soil region of Northeast China. The results showed that the average annual soil erosion modulus in this region was 8.53 t•ha^{-1}•year^{-1}, and the average monthly soil erosion modulus was 0.78 t•ha^{-1}•month^{-1}. The months of April-July and October were identified as critical periods for erosion, with erosion modulus values of 1.17, 1.89, 1.61, 1.13, and 0.93 t•ha^{-1}•month^{-1} during these five months, respectively. High soil erosion was mainly distributed in southern Liaoning province and western Inner Mongolia, and these high erosion areas were mostly distributed in the regions with complex landforms, in grasslands, and in the southern temperate climatic zone. Among multiple driving factors, the topographic factor LS (L = slope length, S = slope steepness) was one of the dominant factors determining the spatial distribution pattern of soil erosion with 30 % of the contribution. The rainfall erosivity (R) and cover management (C) were the major factors driving significantly the intra-annual variation of soil erosion in Northeast China with 27.2 % and 28.9 % of the contribution, respectively. The intra-annual erosion varied with the rainfall and the vegetation growth, and the period of high erosion occurs in the early part of the wet season when the rainfall intensity increases and the vegetation growth is insufficient to protect the soil. Our findings highlight the need to take dynamic factors into consideration in the RUSLE model and the importance for identifying the areas at high erosion risk so as to take soil conservation actions.

1. Introduction

Topsoil nutrient loss and reduced soil fertility caused by soil erosion have serious implications for food, water, and livelihood security (Blaikie and Brookfield, 2015; Obalum et al., 2012). Much work has been done to develop soil erosion models for estimating soil erosion modulus, and one of the most widely used empirical models is the revised universal soil loss equation (RUSLE)(Koirala et al., 2019; Panagos et al., 2014; RENARD et al., 1991). The RUSLE model has been widely used to estimate soil erosion risk, exhibiting sufficient accuracy in large-scale regional studies, and thus it has become an important basic tool for assessing the spatial and temporal variations of soil erosion (Le Roux et al., 2008; Magesh and Chandrasekar, 2016; Polykretis et al., 2020). So far, the RUSLE model has mostly been applied for estimating long-term inter-annual soil erosion variations without considering the intra-annual monthly-scale temporal variation in soil erosion (Fang et al., 2019; Gelagay and Minale, 2016; Polykretis et al., 2020; Sujatha and Sridhar, 2018). When the large-scale C-factor (cover management) is estimated, C-factor values tend to be assigned on the land use map based on the existing literature (Borrelli et al., 2014; De Vente et al., 2009), or calculated using the annual average normalized difference vegetation index (NDVI)(Prasannakumar et al., 2012). This coefficient calculation method masks the intra-annual dynamics of rainfall and vegetation and ignores the intra-annual variation of hydraulic erosion, which is unfavorable for a full understanding of the seasonal or monthly water erosion conditions, especially in the face of study areas with high intra-annual erosion variability.

The black soil region in Northeast China is one of the three major black lands in the world and is the main production area for grain and the largest commercial grain base (Wen and Liang, 2001; Nations AOftU, 1998). Nevertheless, serious soil erosion has occurred due to the long-term large-scale reclamation, thus causing great losses in soil quality

* Corresponding author.
E-mail address: huali@mail.hzau.edu.cn (L. Hua).

https://doi.org/10.1016/j.ecolind.2023.110187
Received 1 January 2023; Received in revised form 5 March 2023; Accepted 23 March 2023
Available online 3 April 2023

and grain production (Xu et al., 2010). Soil erosion in the black soil areas of Northeast China is mainly in the form of water erosion (Fan et al., 2005; Yu et al., 2010), and the main climatic factor affecting runoff and erosion in black soil areas is precipitation (Yang et al., 2003). Northeast China has a predominant temperate monsoon climate with hot rainy summers and cold dry winters. Annual rainfall is characterized by an irregular distribution in time and space, thus leading to great spatio-temporal differences in soil erosion. The vegetation types in the northeast China are diverse, and the vegetation coverage varies greatly within the year. Vegetation coverage is the main factor for reducing erosion, and the vegetation in Northeast China has different resistance to erosion at different time of the year. This natural pattern of precipitation and vegetation growth results in a large temporal and spatial variation of soil erosion over the year (Baiamonte et al., 2019; Humphrey et al., 2022; Panagos et al., 2012). At present, the RUSLE model remains the most suitable method available for evaluating soil erosion in Northeast China which is dominated by water erosion (Feng et al., 2002). However, most soil erosion studies in northeast China focus on annual erosion (Wan et al., 2022; Wang et al., 2020), and few reports on intra-annual hydraulic erosion are available, and even fewer studies have been

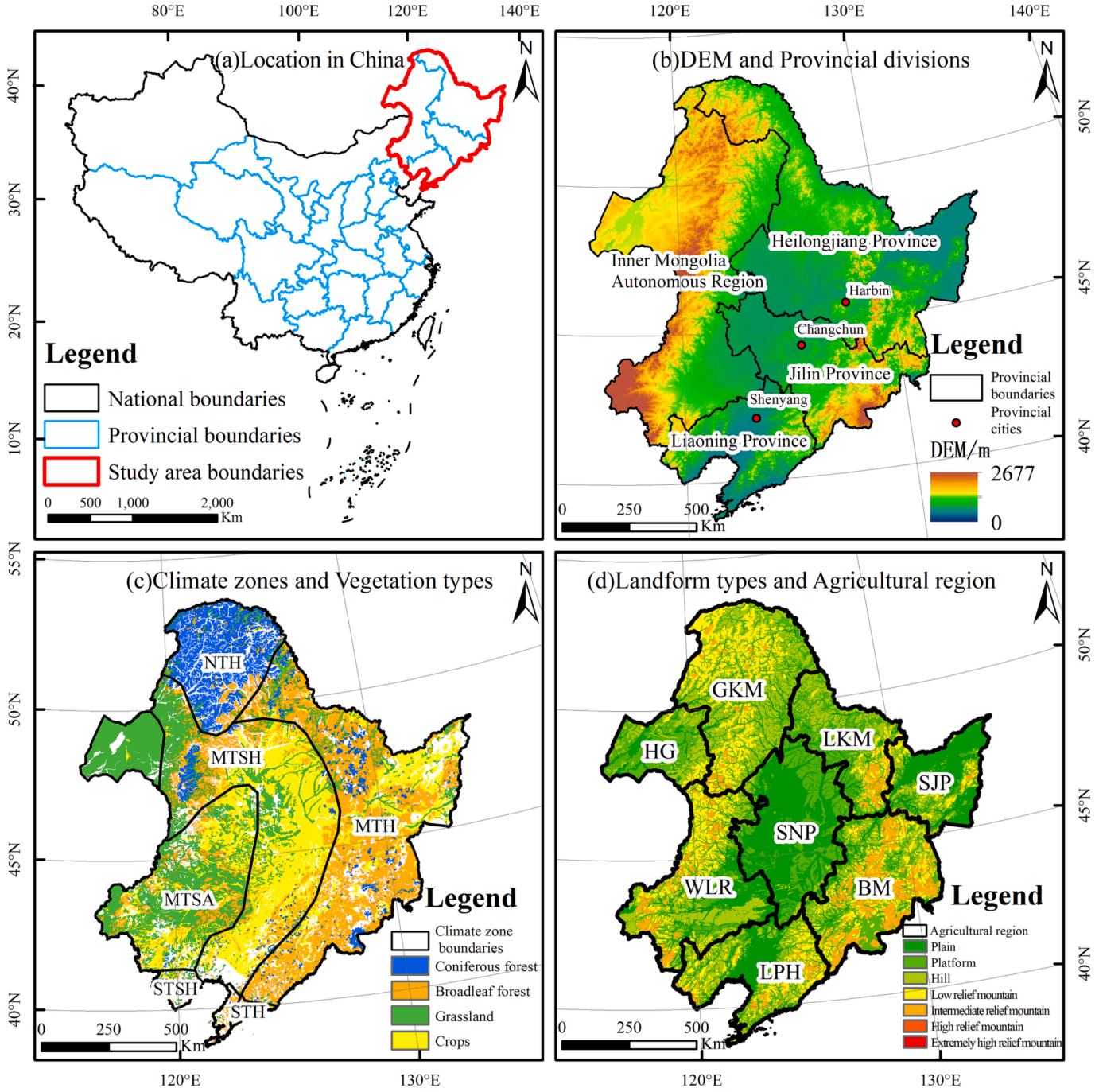

Fig. 1. Overview of study area. (a) location of the study area in China. (b) Digital elevation model (DEM) and provincial divisions. (c) Climate zones and vegetation types. (d) Landform types and agriculture region. NTH, North temperate humid zone; MTH, Middle temperate humid zone; MTSH, Middle temperate sub-humid zone; MTSA, Middle temperate sub-arid zone; STH, South temperate humid zone; STSH, South temperate sub-humid zone; SJP, Sanjiang Plain Zone; GKM, Greater Khingan Mountain Zone; LKM, Lesser Khingan Mountain Zone; BM, Baekdu Mountain Zone; SNP, Songnen Plain Zone; WLR, Western Liao River Zone; HG, Hulunbuir Grassland Zone; LPH, Liaoning Plain and Hilly Zone.

conducted to analyze the drivers of intra-annual water erosion including precipitation and vegetation growth.

Capturing monthly variability in soil erosion models is not a new concept. It has been suggested early that the monthly-scale resolution should be considered in soil erosion modeling (Wischmeier and Smith, 1965). The K (soil erodibility factor), LS, and, P (soil and water conservation measure factor) factors are all relatively static at the time scale, and the temporal variations of the R (rainfall erosivity factor) (Ballabio et al., 2017; Delgado et al., 2022; Johannsen et al., 2022; Shi et al., 2021; Wei et al., 2022) and C factors (Alexandridis et al., 2015; Efthimiou et al., 2022; Schmidt et al., 2018; Yang, 2014) have been studied on a monthly or seasonal basis. Recently, several studies have improved the sensitivity of monthly assessments of soil erosion by exerting the advantages of combining dynamic R and C factors in accurately identifying erosion-prone seasons and areas. For example, (Humphrey et al., 2022) studied dynamic soil erosion rates in Wenham Bay, Kenya, 2017–2020; Schmidt et al.(2019) revealed the monthly risk of soil erosion in Swiss grasslands; Polykretis et al.(2020) explored seasonal soil erosion in different agricultural areas and administrative divisions; and Castro et al. (2022) reported the critical period of greatest seasonal soil loss in the Brazilian Cerrado. However, due to the short time span of most monthly-scale erosion studies, the related results remain to be further verified. In addition, there is still a lack of research on the main controlling factors of monthly soil erosion, and monthly changes in soil erosion tend to be ignored in existing studies. Monthly changes in soil erosion are mainly caused by precipitation and vegetation. Therefore, it is important to understand the complex relationships among precipitation, vegetation, and soil erosion at the pixel scale. In this study, we aimed to assess the intra-annual soil erosion dynamics in black soil regions of Northeast China with the following objectives: (1) to investigate intra-annual spatio-temporal patterns of soil erosion under different spatial units (such as climatic zones and vegetation types) by combining monthly R and C factors; (2) to identify the main factors controlling soil erosion and elucidate the driving effects of R and C factors on erosion changes; and (3) to obtain intra-annual spatial and temporal soil erosion control strategies.

2. Materials and methods

2.1. Study area

The study area is located in the black soil regions of Northeast China including the areas in Liaoning, Jilin, and Heilongjiang provinces in Northeast China and part of the Inner Mongolia Autonomous Region (including Chifeng, Tong Liao, Hulunbeier, and Xing 'an Meng)(Fig. 1). The vegetation types in the study area are diverse mainly including broad-leaved forests, coniferous forests, grasslands, and crops. The terrain in the study area is diverse containing a variety of topographical features such as plains, mountains, and low hills. The western, eastern, and southern parts of the study area are surrounded by mountains on three sides, namely, the Daxinganling, Xiaoxinganling, and Changbai Mountains, and the three mountain ranges surround the Songnun Plain and the Liaohe Plain. The study area has a temperate monsoon climate with heavy rainfall in summer, which is likely to cause water erosion. In general, the rainy season occurs from June to September, with the onset of the rainy season occurring earlier in the southern region, typically around April. The vegetation growth season usually starts in April and ends in September.

2.2. Data collection

To estimate the various factors of RUSLE, various datasets were collected in this study. These datasets contain meteorological data, satellite images, soil properties, topography, and land use data (Table 1). Data were pre-processed using the software such as Excel, ArcGIS, and MATLAB.

Table 1
Datasets used in this study.

Data	Source	Resolution
Daily station observation data of Chinese meteorological elements	the Resource and Environment Science and Data Center (https://www.resdc.cn/)	/
MODIS-MOD13Q1 product (provides the Normalized Difference Vegetation Index)	NASA	250 *m*
Digital elevation model (DEM)	the Resource and Environment Science and Data Center (https://www.resdc.cn/)	30 *m*
The 30 m annual land cover dataset in China from 1990 to 2019 (Annual China Land Cover Dataset, CLCD)	Zendo (https://zenodo.org/)	30 *m*
Basic attribute data of China High Resolution National Soil Information Grid (2010–2018)	Soil Science Data Center, Institute of Soil Science, Chinese Academy of Sciences (https://data.issas.ac.cn/)	90 *m*

2.3. RUSLE model

Water erosion is one of the most important factors causing soil erosion in Northeast China, and it is accurately quantified by the RUSLE (Phinzi and Ngetar, 2019). Soil erosion assessment is performed in ArcGIS (10.7) using RUSLE, and it is calculated according to the following Eq. (1)

$$A = R{\cdot}K{\cdot}LS{\cdot}C{\cdot}P \tag{1}$$

where A is the average annual soil loss ($t{\bullet}ha^{-1}{\bullet}year^{-1}$); R is the rainfall erosivity factor ($MJ{\bullet}mm{\bullet}ha^{-1}{\bullet}h^{-1}{\bullet}year^{-1}$); K is the soil erodibility factor ($t{\bullet}ha{\bullet}h{\bullet}ha^{-1}{\bullet}MJ^{-1}{\bullet}mm^{-1}$); LS is the slope length and steepness factor (dimensionless); C is the cover management factor (dimensionless, ranging from 0 to 1); and P is the soil and water conservation measure factor (dimensionless, ranging from 0 to 1). Eq. (2) can be used to calculate the monthly soil loss status ($t{\bullet}ha^{-1}{\bullet}month^{-1}$) by modifying the temporal resolution of dynamic factors R and C from year to month (Eq. (2)) (Humphrey et al., 2022; Renard, 1997; Schmidt et al., 2019)

$$A_{month} = \mathrm{R}_{month} \bullet K \bullet LS \bullet \mathrm{C}_{month} \bullet P \tag{2}$$

In this study, monthly soil erosion was calculated as monthly soil erosion modulus based on a long time series from 2001 to 2019 in each year, and then the multi-year monthly average soil erosion modulus (Eq (3)) was calculated according to Eq. (3)

$$\overline{A}_{month} = \frac{\sum_i^n A_{month}}{19} \tag{3}$$

where, n indicate year number from 2001 to 2019.

As for the resolution, we resampled all factor result to a common spatial resolution of 30 m × 30 m. Based on this, soil erosion results were obtained at 30 m resolution (Fig. 3). The distribution of first and maximum erosion months at 30 m resolution was also calculated by the raster calculator tool of ArcMap 10.7 (Fig. 5).

2.4. Rainfall erosivity factor (R)

The rainfall erosivity factor (R) reflects the effect of rainfall intensity on soil erosion. In this study, the erosion force was calculated by daily rainfall model based on the daily rainfall data from Chinese meteorological stations, as previously reported (Zhang and Fu, 2003). The semi-monthly erosion force was calculated according to Eq. (4) (Zhang et al., 2002). After calculating the rainfall erosivity factor at each meteorological station, the results were kriged interpolated with a spatial resolution of 1 km and resampled to 30 m.

$$R_j = \alpha \sum_{j=1}^{k} (P_d)^{\beta}$$

$$\beta = 0.8363 + \frac{18.177}{P_{d12}} + \frac{24.455}{P_{y12}} \quad (4)$$

$$\alpha = 21.586\beta^{-7.1891}$$

where R_j is the semi-monthly erosion force (MJ•mm/ hm^2•h); k is the number of days (d) in the semi-monthly period; Pd is the daily rainfall (mm) (Pd ≥ 12 mm); λandβare model parameters; P_{d12} is the average daily rainfall (mm) for the days with a daily rainfall ≥ 12 mm; and P_{y12} is the average annual rainfall (mm) for the days with a daily rainfall ≥ 12 mm.

2.5. Soil erodibility factor (K)

Soil erodibility factor (K) was calculated based on soil property data from Soil Science Data Center, Institute of Soil Science, Chinese Academy of Sciences by EPIC model (erosion-productivity impact calculator) according to Eq. (5) (William and Arnold, 1993; Williams et al., 1983):

$$K = \left\{0.2 + 0.3exp\left[-\frac{0.0256Sand(1-Silt)}{100}\right]\right\} \times \left(\frac{Silt}{Clay+Silt}\right)^{0.3} \times \left[1.0 - \frac{0.25SOC}{SOC + exp(3,718 - 2.947SOC)}\right] \times \left[1.0 - \frac{0.7SN1}{SN1 + \exp(-5.509 + 22.899SN1)}\right] \quad (5)$$

where K is soil erodibility factor (t ha h/MJ mm^{-1} ha^{-1}); SOC is the soil organic carbon content (%); sand, silt, and clay represent the soil sand content (particle size within 0.05 mm-2 mm, %), silt content (particle size within 0.002 mm-0.05 mm, %), and clay content (particle size < 0.002 mm, %), respectively. *SN*1 was calculated as 1 − Sand/100.

2.6. Topographic factor (LS)

The topographic factor is used to quantify the effect of topography on soil erosion, and it is calculated by digital elevation model (DEM) with a resolution of 30 m using Fu Suhua's LS calculation tool (Fu et al., 2015).

2.7. Cover management factor (C)

The cover management factor C is an important indicator of vegetation erosion resistance, and the areas with high vegetation cover tend to have a relatively low probability of soil erosion occurrence. The Eq. (6) reflects the inhibitory effect of factor C on soil erosion. In this study, the C factor was calculated by the method proposed by Cai et al.(2000). The vegetation cover is calculated by Eq. (7).

$$c = 1, 0 \le f_c\% < 0.1$$

$$c = 0.6508 - 0.3436\lg(f_c\%), 0.1 \le f_c\% \le 78.3$$
$$c = 0, f_c\% > 78.3 \quad (6)$$

$$f_c\% = \frac{NDVI - NDVI_s}{NDVI_v - NDVI_s} \quad (7)$$

where fc% is the vegetation cover, $NDVI_s$ and $NDVI_v$ are the NDVI values for pure bare soil pixels, and pure vegetation pixels respectively.

2.8. Soil and water conservation measure factor (P)

The soil and water conservation measure factor P reflects the effect of soil and water conservation measures on the amount of soil erosion, and P factor is usually assigned a value according to the type of land use, and the specific value assignment in this study was shown in the Table 2.

Table 2
Value assignment of P factor for different land uses.

Land Use Type	P-value
Water area, impermeable layer	0
Water field	0.01
Dry land	0.25
Others	1

2.9. Main controlling factor assessment by random forest and change decomposition analysis by LMDI model

A random forest is a compositional supervised learning method, and it can be considered as an extension of decision trees. When the response variables are a set of categorical variables representing the grouping information of the samples, the random forest is used to perform the function of supervised classification, while when the response variables are a set of continuous variables, the random forest can be used for regression analysis to effectively assess the importance of the variables and identify the dominant factors in soil erosion, which is conducted through the Random Forest package in R (version R 4.3.3).

The logarithmic mean Divisia index (LMDI) method is an important method to quantify the influence of different factors on dependent variables, and LMDI can explain the reason for the change of dependent variables by decomposing the effects of each factor (Ang, 2004; Ang, 2005; Ang, 2015). Since the structure of RUSLE is consistent with that of LMDI, it is valid and reliable to use the LMDI model for the analysis of soil erosion changes. The contribution values of R and C factors to monthly soil erosion changes were calculated at the 30 m pixel scale by the additive decomposition of LMDI and RUSLE models (Fig. 8 and Fig. 9), and the calculation equations were as follows (He et al., 2020).

$$\Delta A_R = \sum_i^n \frac{\left(A_i^m - A_i^{m-1}\right)}{\left(lnA_i^m - lnA_i^{m-1}\right)} \ln\left(\frac{R_{k,i}^m}{R_{k,i}^{m-1}}\right) \quad (8)$$

$$\Delta A_C = \sum_i^n \frac{\left(A_i^m - A_i^{m-1}\right)}{\left(lnA_i^m - lnA_i^{m-1}\right)} \ln\left(\frac{C_{k,i}^m}{C_{k,i}^{m-1}}\right) \quad (9)$$

where ΔAC is the contribution of C-factor to soil erosion change (t/hm2-a); ΔAR is the contribution of R-factor to soil erosion change (t/hm2-a); A_i^m is the m^{th} month soil erosion modulus (t/(hm2-a)); A_i^{m-1} is the *m*-1th month soil erosion modulus (t/(hm2-a)); $C_{k,i}^m$ is the m^{th} month vegetation cover factor; $C_{k,i}^{m-1}$ is the *m*-1th month vegetation cover factor; $R_{k,i}^m$ is the m^{th} month rainfall erosion force factor; and$R_{k,i}^{m-1}$ is the *m*-1th month rainfall erosion force factor. $\Delta A_C > 0$ or $\Delta A_R > 0$ indicates that the C factor or R factor aggravates soil erosion. $\Delta A_C < 0$ or $\Delta A_R < 0$ indicates that the C factor or R factor mitigates soil erosion. Since each factor in the RUSLE model has no subset, the value of n in the equation is equal to 1.

To better understand the impact of both the C factor and the R factor on soil erosion, we have combined the values of ΔA, ΔAC, and ΔAR, resulting in a total of six different schemes (Table 3). Results are

Table 3
Relative effects of C factor and R factor on soil erosion variation.

ΔA	ΔAC	ΔAR	Description
>0	>0	>0	Increased soil erosion under the joint actions of C factor and the R factor (IECR)
	>0	<0	Increased soil erosion caused by C factor alone (IEC)
	<0	>0	Increased soil erosion caused by R factor alone (IER)
<0	<0	<0	Decreased soil erosion under the joint actions of C factor and the R factor (DECR)
	<0	>0	Decreased soil erosion caused by C factor alone (DEC)
	>0	<0	Decreased soil erosion caused by R factor alone (DER)

displayed at a resolution of 30 m (Fig. 11).

3. Results

3.1. Monthly average soil erosion status and its regularity in Northeast China

3.1.1. Monthly average soil erosion in Northeast China

Multi-year monthly average soil erosion modulus at a resolution of 30 m was calculated by RUSLE model to reveal soil loss in Northeast China from 2001 to 2019 (Figs. 2 and 3). Our results showed that the multi-year annual average soil erosion modulus in the study area was 8.53 t•ha^{-1}•year^{-1}, which was similar to one previous report on multi-year annual average soil erosion modulus (8.93 t•ha^{-1}•year^{-1})(Wang et al., 2021), confirming the reliability of our results.

The spatial distribution results showed that the south (along with part of the east) and west were high erosion risk areas, and that the high erosion risks in these areas might be related to topography, rainfall, and vegetation. The spatial soil erosion patterns in Northeast China in this study were similar to those reported by Fang and Fan (2020) and Wan et al. (2022). The high erosion risk areas are mostly characterized by the large number of mountains, and this steep topography creates favorable conditions for erosion (Beskow et al., 2009; Sun et al., 2014; Tiruwa et al., 2021). In terms of timing, January tended to have no soil erosion due to the absence of erosive rainfall occurrence (12 mm) and below-zero temperature. From February to November, the study area exhibited interesting spatial and temporal variation in soil erosion. From February to May, erosion radiated from south to north. From June, erosion decreased in the north with the main erosion concentrated in the southwest. From October to November, severe erosion again occurred in the southeast. The time of high risk in the south was not consistent with that in the west. From February to April, inadequate vegetation coverage and the first erosive rainfall arrival in the south led to severe soil erosion. During the heavy rainfall season from June to August, the woodlands with dense vegetation in the south formed great erosion resistance. The erosion resistance of western grasslands was lower than the erosion force brought by heavy rainfall, in turn producing severe erosion. With the decline in erosive rainfall and the withering of vegetation, the south was subjected to severe soil erosion again in October.

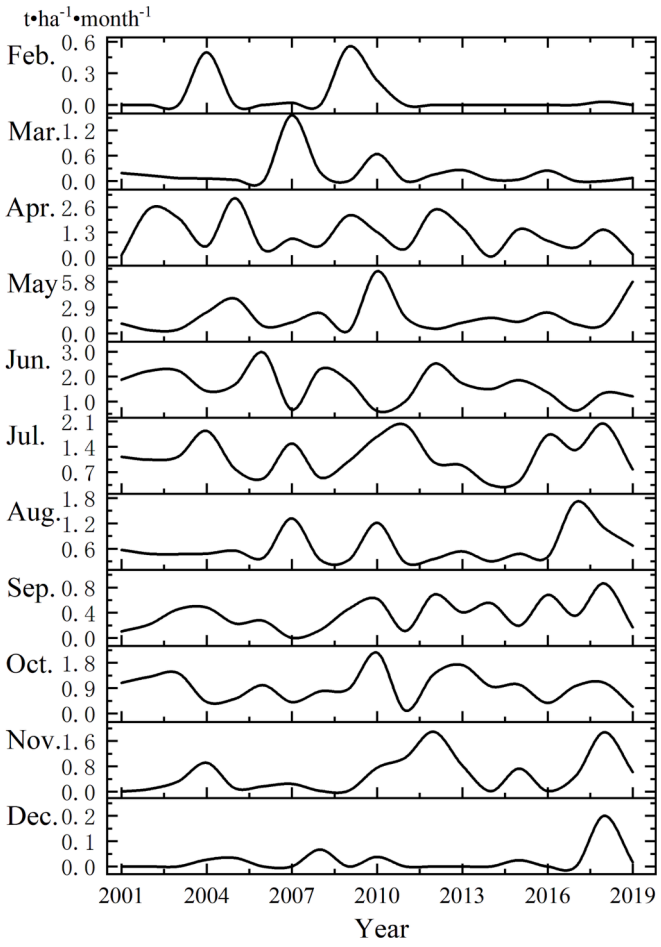

Fig. 2. Monthly soil water erosion modulus from 2001 to 2019.

Moreover, calculating the multi-year monthly average soil erosion modulus in different agricultural zones revealed that values for the Liaoning Plain and Hilly Zone (LPH), the Western Liao River Zone (WLR) and Baekdu Mountain Zone (BM) were the highest, reaching 24.96 t•ha^{-1}•year^{-1},16.37 t•ha^{-1}•year^{-1}and 10.45 t•ha^{-1}•year^{-1}, respectively (Table 4). Interestingly, these three most severely eroded agricultural zones have different temporal patterns throughout the year. The LPH exhibited the earliest onset of erosion and also the earliest peak, with significant erosion occurring in March and reaching its peak in April. A second peak of erosion was also evident in October. As the area with the most severe erosion, the high-risk erosion months for this region are April, May, June, July, October, and November. The erosion patterns in BM and LPH were similar, but the first erosion peak occurred one month later, with two erosion peaks occurring in May and October. Its high-risk erosion months are April, May, October, and November. The erosion in WLR appeared later (in April) and peaks later (in June) than the other two regions, and there was only one peak in erosion during the year. Its high-risk erosion months were also relatively unique, covering the entire summer season from May to August.

As shown in Fig. 4, April to July and October exhibited a relatively high monthly water erosion modulus, and thus these 5 months were identified as high erosion risk periods. Considering this, the erosion control should be enhanced during these 5 months. The average monthly soil erosion modulus was 0.78 t•ha^{-1}•month^{-1} with highest erosion modulus value observed in May (1.89 t•ha^{-1}•month^{-1}) and the lowest value in December (0.02 t•ha^{-1}•month^{-1}) in the study area. These results indicated that erosion was more severe in spring and summer, with a peak erosion period in October during autumn, and the erosion risk was low (nearly zero) in winter. After observing the monthly variations in soil erosion, R factor and C factor. R factor and C factor exhibited completely opposite variation characteristics, reaching their respective maximum value and minimum value in July and August, and that both R factor and C factor showed a single peak characteristic. This was quite different from the variation characteristics of the soil erosion modulus, indicating that both R factor and C factor jointly affected the soil erosion in the study area.

To investigate the spatial and temporal distribution of soil erosion in the study area, we identified the first erosion month and the maximum erosion month (Fig. 5). The first erosion month was distributed from February to May, and the first erosion month came earlier in the south than in the north. The first erosion month occurred in February for the south, in March for the east, in April for the north and west, and in May for the central Sonnen Plain area. The spatial distribution pattern of the first erosion month was primarily influenced by the first erosive rainfall, followed by the anthropogenic measures and topography. The maximum erosion month came earlier in the south than in the north, and earlier in the east than in the west, and the maximum erosion months distributed in the following order: April in the south, May in the north and parts of the east, June in the central plain, July in the west, and October and November in the parts of the east. The occurrence of maximum erosion resulted from the joint spatial and temporal actions of vegetation growth period, vegetation type, rainfall intensity, and climate zone type.

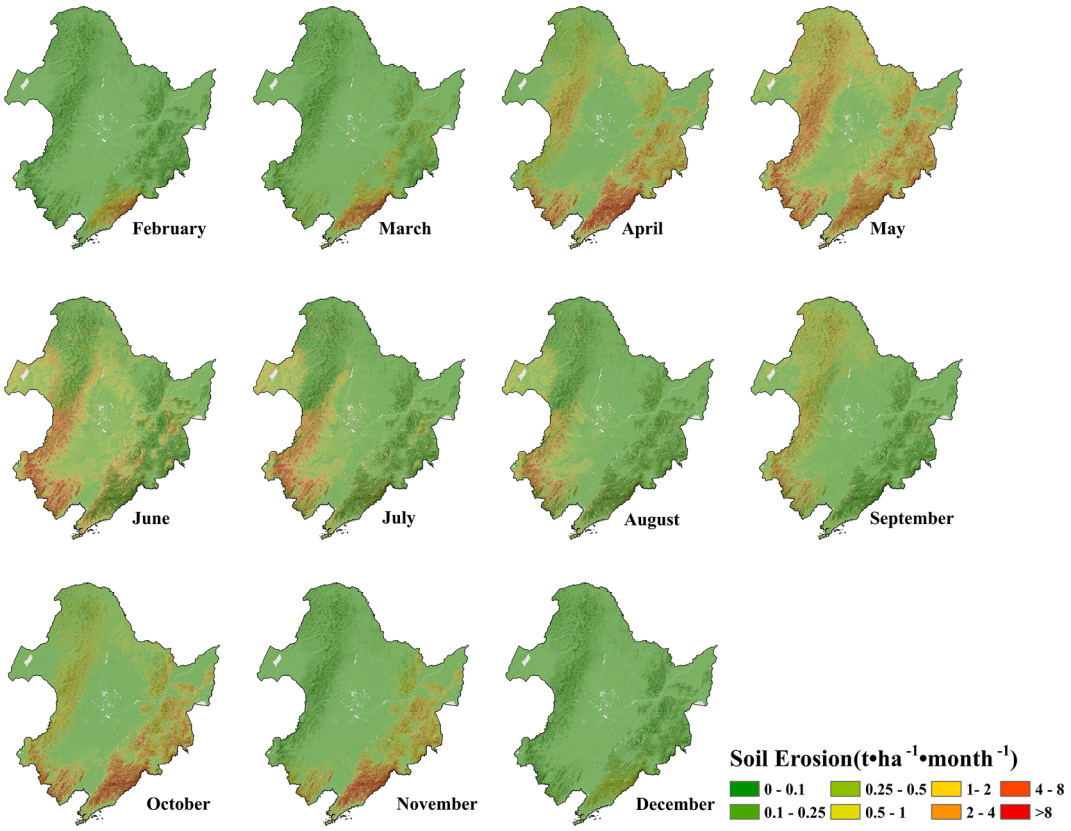

Fig. 3. Monthly average of soil erosion in Northeast China from 2001 to 2019.

3.1.2. Regularity of landform, climatic zone, and vegetation type on monthly erosion

The spatial and temporal distribution of soil erosion during the year was closely related to rainfall, vegetation, and topography. Therefore, climate zones, vegetation types, and landform types were used as spatial units for further analysis of soil erosion regularity (Fig. 6). The erosion modulus varies significantly among different landform types, with mountains being higher than plain and platform, and high relief mountains being higher than low-relief mountains. Especially in July and August, the erosion modulus of high-relief mountains is 2.8 times that of low-relief mountains, and 12 times that of plain and platform.

The erosion modulus exhibited a descending pattern from south to north, ranking in the following order: the southern temperate erosion modulus > the middle temperate erosion modulus > the northern temperate erosion modulus. In the east–west direction, the erosion modulus decreased from east to west during the rainy season, and decreased from west to east during the dry season. The soil erosion peak under different climatic zones occurred in an early-to-late order of southern temperate humid climate > middle temperate humid climate > northern temperate humid climate > middle temperate sub-humid climate > southern temperate sub-humid climate > middle temperate subarid climate. The erosion modulus also differed among vegetation types. Grasslands had the highest erosion modulus, which might be related to their low vegetation coverage (Yan et al., 2003). Broadleaf forests and coniferous forests have their erosion peaks in May, while crops and grasslands have their erosion peaks in June. In October, the second peak of broad-leaved forest and grasslands occurred. The soil erosion peak under different vegetation types occurred in an early-to-late order of broadleaf forest > coniferous forest > crops > grassland.

3.2. The contributions of erosion factors to soil erosion and its variations

3.2.1. Monthly contributions of erosion Factors

To examine monthly contribution of erosion factors in Northeast China, the relative importance of erosion factors obtained based on the random forest method were plotted (Fig. 7). The relative importance of the static factors was relatively stable. Of these static factors, the LS factor was the core erosion controlling factor in the Northeast China with a contribution of about 30 % throughout the year. The LS factor, which reflects the combined effect of slope length and steepness. A steeper slope increases the velocity of runoff water and enhances soil detachment and transport, while a longer slope length increases the volume of runoff and the distance that eroded soil particles can be transported. P factor and K factor had less importance, and they were less influential factors. The dynamic factors varied significantly seasonally and became the main controlling factor of soil erosion successively with the change of rainy and dry seasons. The R-factor was more influential before May and after September, making a contribution of about 27.2 %. The C-factor was more influential from May to September, making a contribution of about 28.9 %.

3.2.2. Contribution of R-factor and C-factor to erosion change in Northeast China

In terms of temporal changes, it is the dynamic factors that cause soil erosion variations. Therefore, it is essential to clarify the changes in dynamic factors (R factor and C factor) and their contribution to the soil erosion variation. The spatial distribution of erosion changes respectively caused by R-factor and C-factor in the study area was investigated by the additive decomposition of LMDI model (Fig. 8 and Fig. 9). As shown in Fig. 8 from February to July, nearly all the space took on red color, indicating that the increasing rainfall aggravated erosion. The increased precipitation led to increased erosion in the south from March to April, throughout the northeast from April to May, in the west from

Table 4
Soil erosion modulus in different agricultural zones.

Month	LPH(t•ha^{-1}•month^{-1})	LKM(t•ha^{-1}•month^{-1})	SJP(t•ha^{-1}•month^{-1})	BM(t•ha^{-1}•month^{-1})	SNP(t•ha^{-1}•month^{-1})	HG(t•ha^{-1}•month^{-1})	GKM(t•ha^{-1}•month^{-1})	WLR(t•ha^{-1}•month^{-1})
2	0.44	0.00	0.00	0.13	0.00	0.00	0.00	0.00
3	1.15	0.02	0.04	0.33	0.00	0.00	0.00	0.01
4	5.18	0.37	0.39	2.04	0.06	0.19	0.45	0.70
5	4.04	0.99	0.80	2.70	0.25	0.72	1.77	2.91
6	3.86	0.25	0.24	1.10	0.41	0.94	0.51	4.68
7	1.97	0.08	0.10	0.51	0.17	0.77	0.19	4.37
8	1.47	0.07	0.07	0.35	0.07	0.43	0.10	2.05
9	0.47	0.13	0.05	0.09	0.03	0.28	0.56	0.88
10	3.49	0.30	0.53	1.87	0.04	0.08	0.32	0.71
11	2.77	0.10	0.31	1.28	0.01	0.00	0.00	0.05
12	0.12	0.00	0.00	0.04	0.00	0.00	0.00	0.00
Total	24.96	2.33	2.52	10.45	1.05	3.42	3.90	16.37

May to June, suggesting that erosion control measures should be taken in these areas. There appeared a turning point in July-August when rainfall made a slight positive contribution to erosion in the south, but it started to make a negative contribution in other regions. From August to December, the contribution diagram of R factor almost took on green color, indicating reduced rainfall resulted in decrease in the erosion (Fig. 8). As time progressed from August to December, the west, the north, the southeast, and the south areas successively became the maximum areas of negative contribution.

Vegetation is one of the most important environmental factors controlling soil erosion (Lieskovský and Kenderessy, 2014). Vegetation can protect soil against erosion by preventing surface runoff, and thus it has an important role in soil conservation. In this study, NDVI was used to determine the C-factor, and the C-factor and vegetation growth were directly related. From February to June, the excellent vegetation growth status in the study area made a negative contribution to the region-wide erosion modulus change (Fig. 9). This negative contribution gradually increased from south to north over time. From September to December, due to vegetation withering, the C factor made a positive contribution to erosion modulus change. The period from June to September exhibited both negative and positive contributions of vegetation to erosion modulus, which might be attributed to the difference in timing of different vegetation withering periods.

3.2.3. Contributions of R-factor and C-factor to soil erosion change in Northeast China under different spatial units

Fig. 10 is the contribution of R-factor and C-factor to erosion change under different spatial units. The results showed that R-factor produced the lowest erosion contribution in the north temperate zone and the highest in the south temperate zone. In July-August, due to the long rainstorm season in the southern temperate zone, rainfall in the southern temperate zone continuously provided a positive contribution to erosion modulus change, whereas in July-August, the positive contribution turned into the negative contribution in the northern and middle temperate zones. Different humid zones within the same temperate zone also had different patterns at different times. Specifically, the sub-humid and sub-arid zones had a greater contribution to erosion change during the rainy season, and the humid zones had a greater contribution to erosion change during the non-rainy season. The results provided useful reference for erosion control in different climatic zones in response to rainfall changes. The contribution of C-factors to erosion change varied with time. The grasslands and crops contributed more to erosion change during the summer months, whereas woodlands, especially broadleaf forests, contributed more to erosion change during other seasons. This regularity of erosion contribution of different vegetation had a certain implication for the selection of vegetation types and the optimization of mixed planting patterns.

3.3. R factor versus C factor in monthly erosion change

Our findings suggest that the increase in rainfall before June was the primary cause of erosion increase (Fig. 11). From April to July, the radiation of the green area (DEC) from south to north reflected the decrease in erosion due to the increased vegetation resistance to erosion. Over time, the diffusion of DEC from south to north was related to vegetation types and their greening period. The greening period of broadleaf forest in the south occurred earlier than that of coniferous forest in the north, and earlier than that of crops in the central region. Therefore, the areas where erosion decreased due to vegetation appeared successively from south to north. In July and August, the joint effect of rainfall and vegetation resulted in a decrease in erosion. From August to November, the radiation of the yellow area (IEC) from north to south reflected the intensified erosion due to the decreased vegetation coverage, which is also the reason for the second peak of erosion in October in the Northeast region. erosion increase before crop vegetation cover is sufficient and after the arrival of forest withering period.

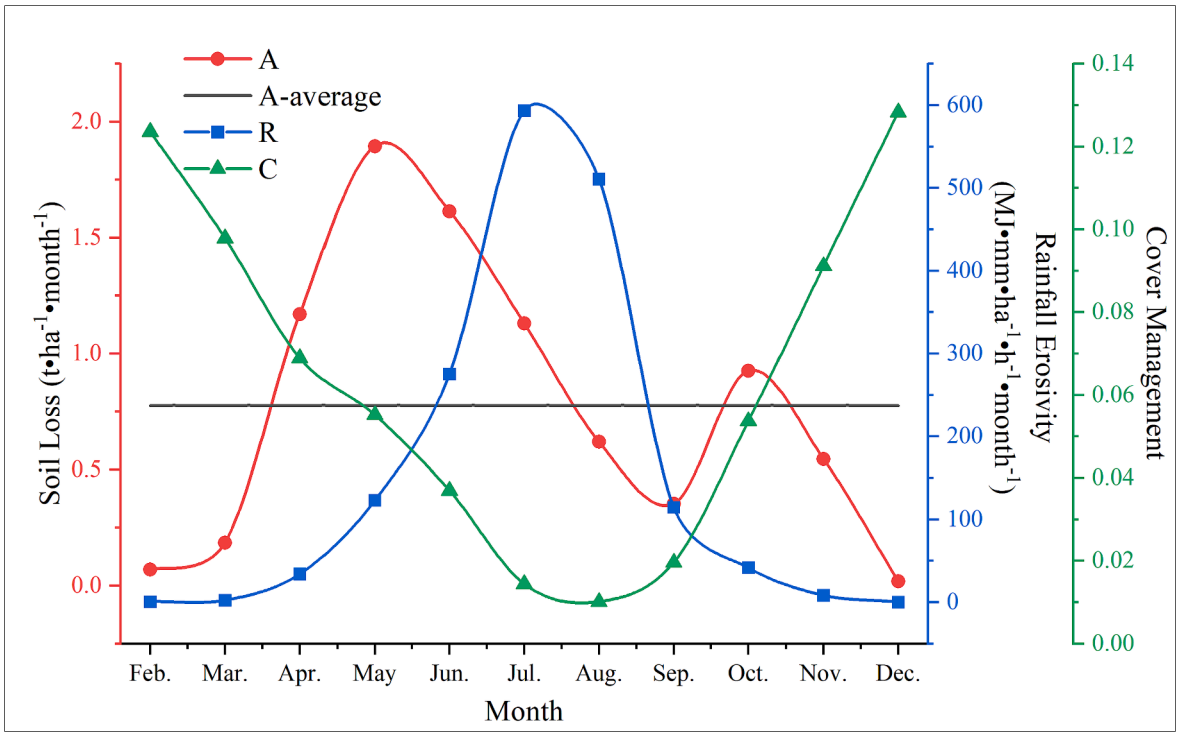

Fig. 4. Monthly soil erosion modulus and influencing factors within a year. A, soil erosion modulus; A-average, monthly average soil erosion modulus; R, rainfall erosivity factor; and C, cover management.

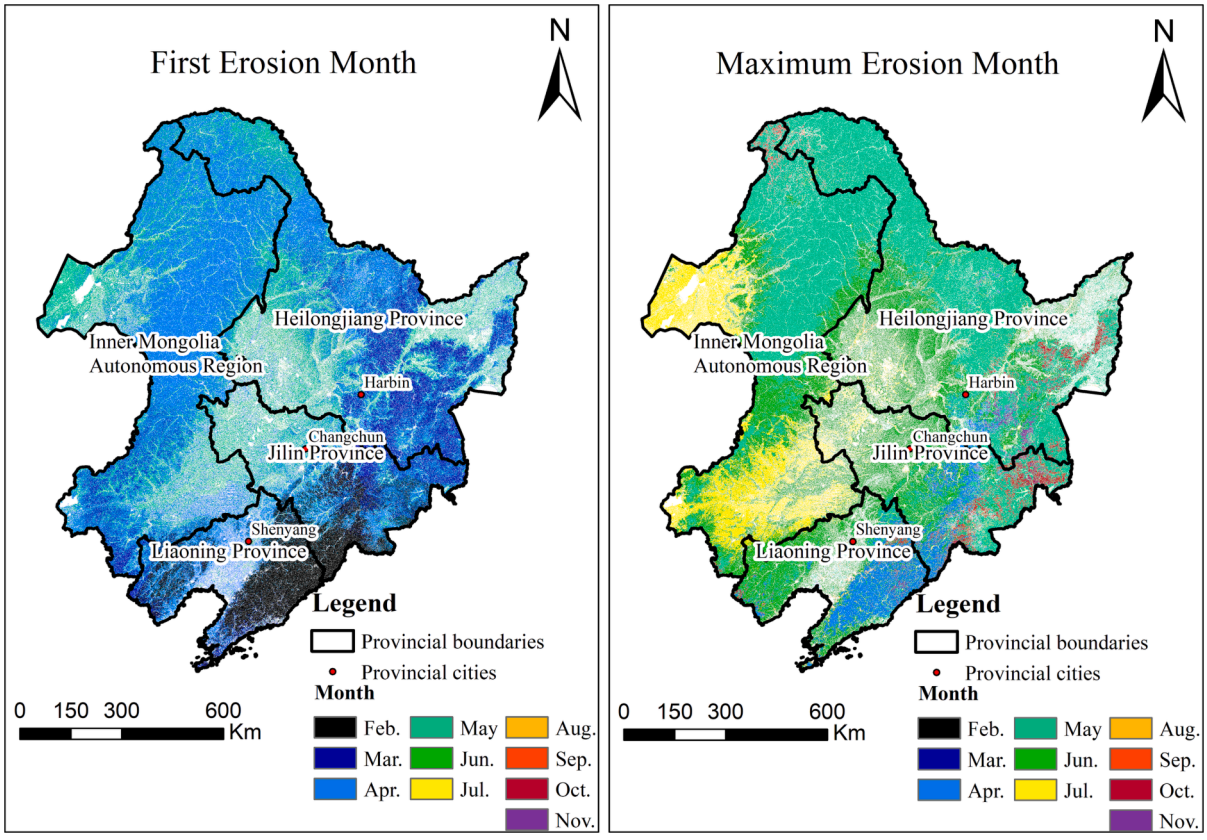

Fig. 5. First erosion month and Maximum erosion month.

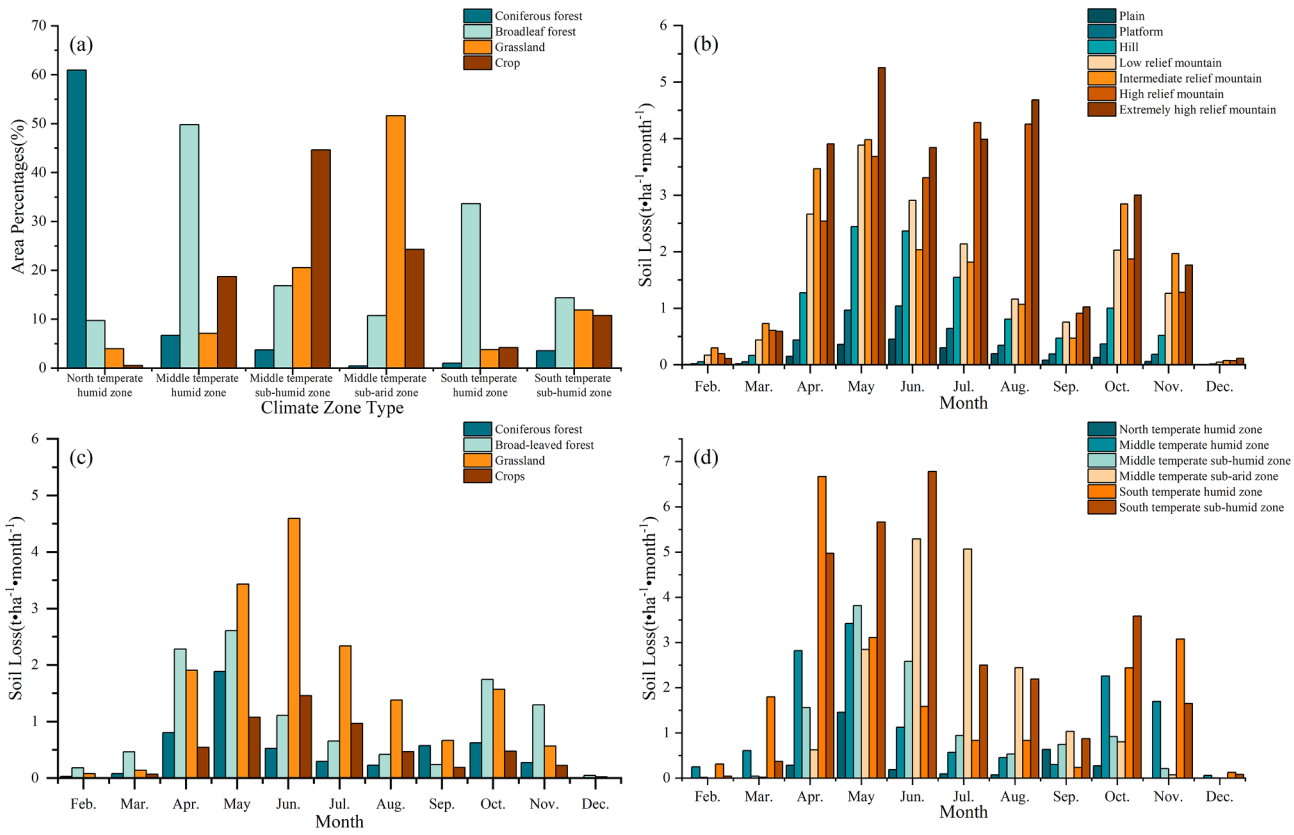

Fig. 6. Erosion status of different spatial units in Northeast China. (a) Percentages of different vegetation types in different climatic zones. (b) Soil erosion histogram under different landforms from February to December. (c) Erosion histogram under different vegetation types from February to December. (d) Erosion histogram in different climatic zones from February to December.

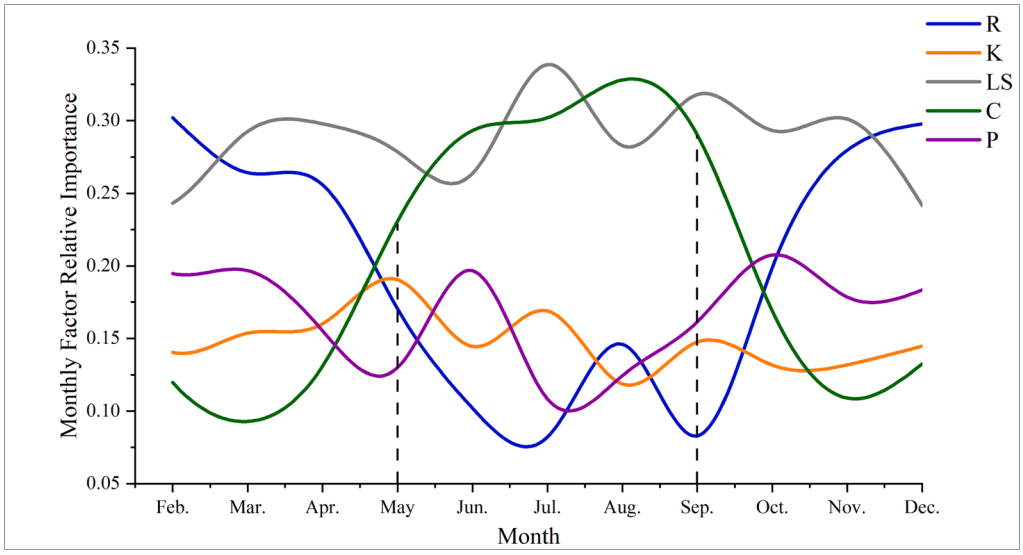

Fig. 7. Monthly contribution of erosion factors.

4. Discussion

4.1. Determining the period of high erosion risk

Applying dynamic R and C factors to evaluate soil erosion can facilitate the accurate identification of high-risk periods for monthly soil erosion. In some studies, the R factor is considered to be the most influential factor responsible for the intra-annual soil erosion dynamics (Polykretis et al., 2020; Schmidt et al., 2019). Their studies shows that the period with the highest R factor is the month with the greatest soil erosion. Our results showed that the soil erosion in the study area was not controlled by the R factor or C factor alone (Fig. 4). Either heavy rainfall alone (high R factor value) or low vegetation cover alone (high C factor value) did not lead to severe erosion. The most vulnerable period to erosion was the early wet season when rainfall intensity was increasing but vegetation growth was not sufficient to protect the soil,

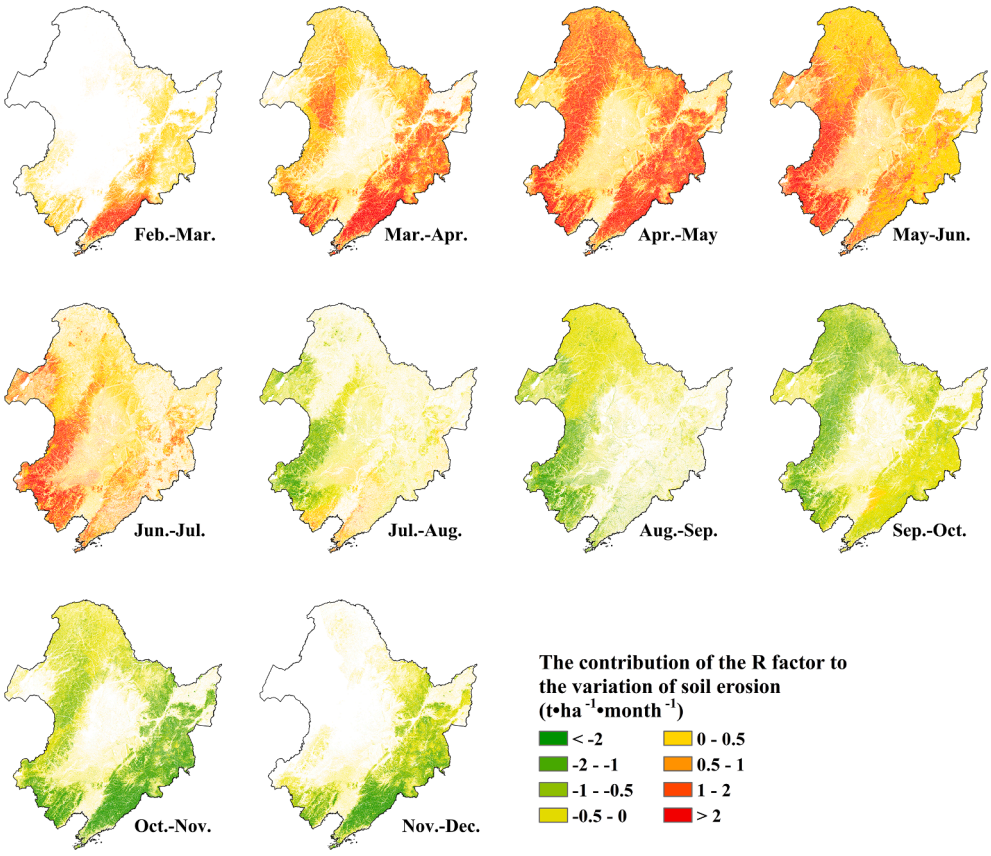

Fig. 8. Contribution of R factor to soil erosion.

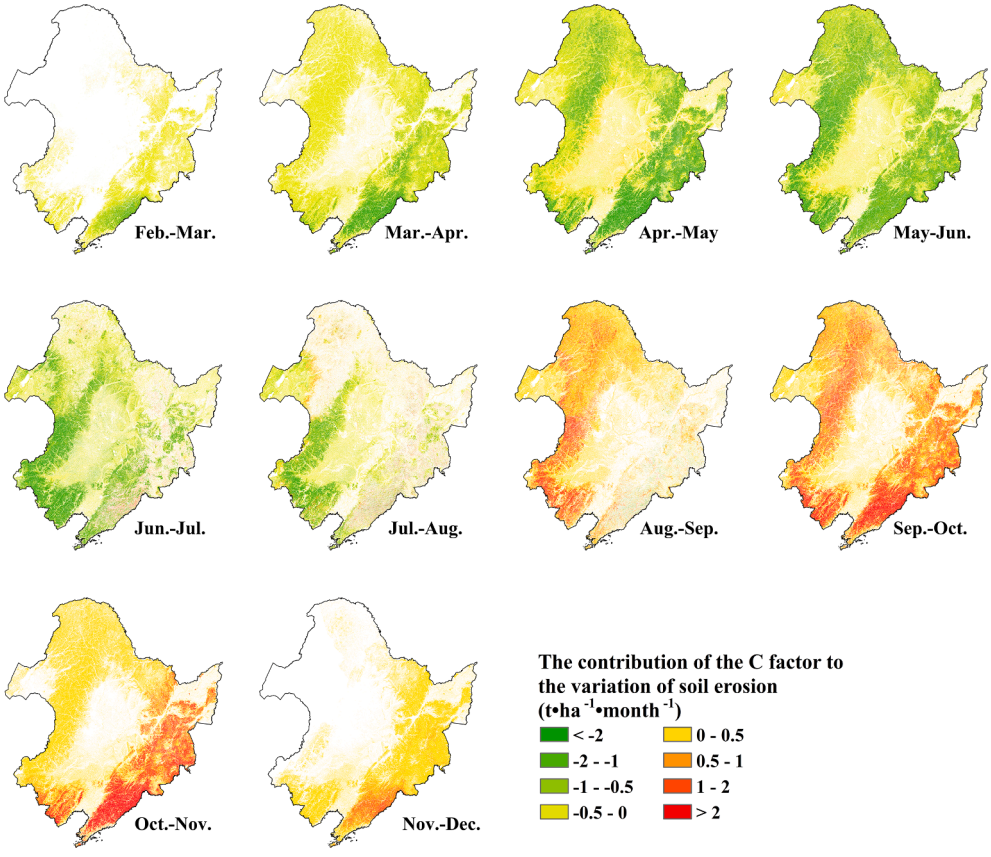

Fig. 9. Contribution of C factor to soil erosion variation.

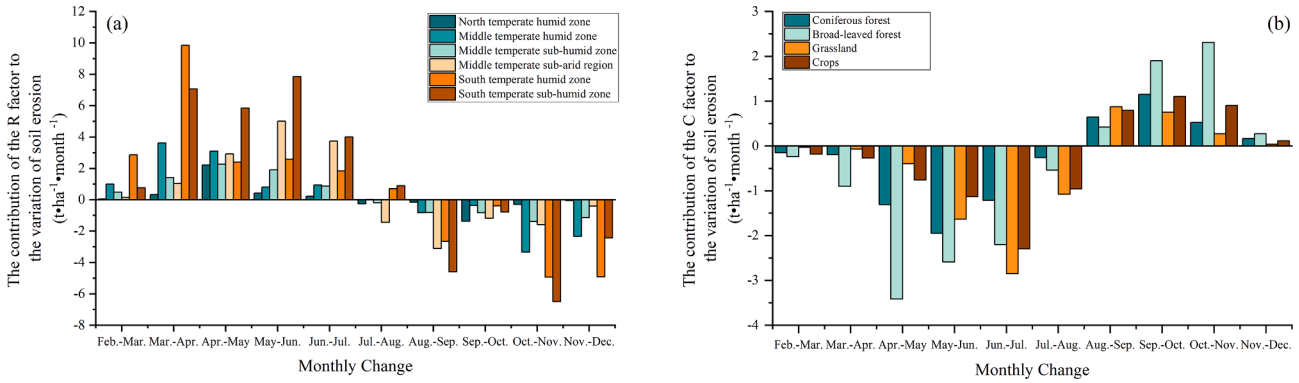

Fig. 10. Contribution of R-factor and C-factor to erosion change under different spatial units. (a) Contribution of R-factor to erosion change in different climatic zones. (b) Contribution of C factor to erosion changes under different vegetation types.

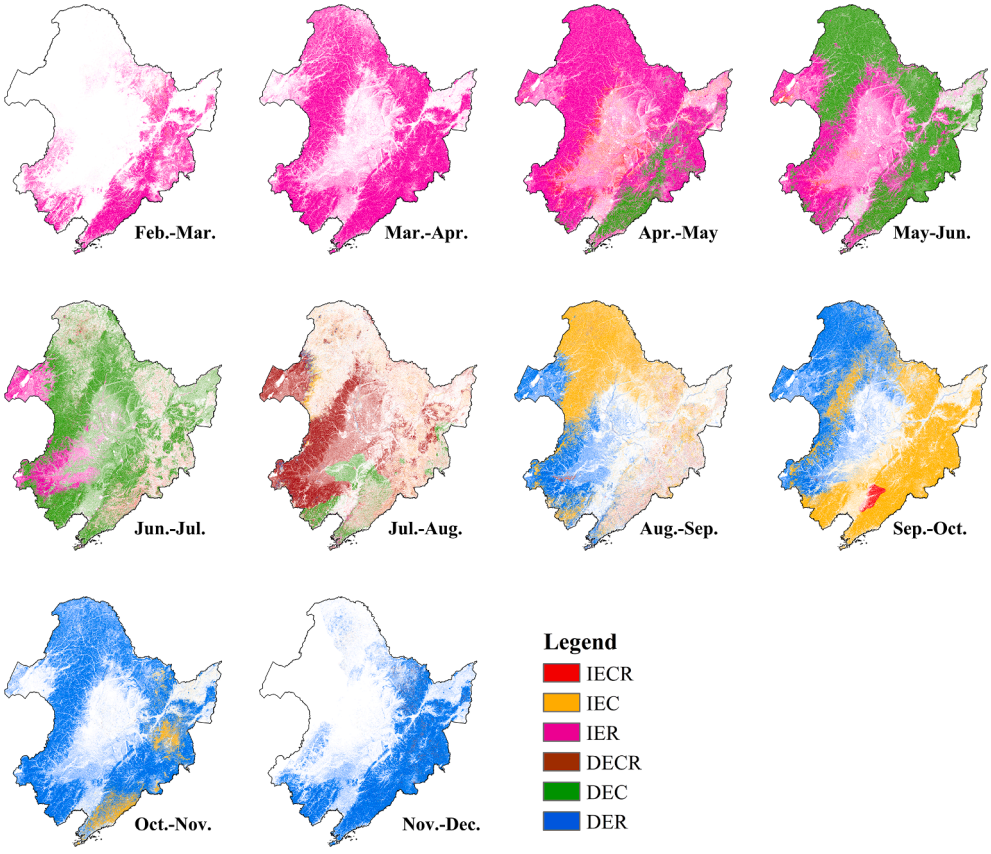

Fig. 11. Drivers of monthly erosion change. Note: C factor, vegetation cover factor; R factor, rainfall erosivity factor; ΔA, the variation of soil erosion; ΔAC, contribution of C factor to soil erosion variation.; ΔAR, contribution of R factor to soil erosion variation.

and thus erosion peak preceded rainfall peak, suggesting the erosion effect brought by the lagging of vegetation growth (Humphrey et al., 2022).

Interestingly, unlike the single-peak characteristics of the monthly erosion in previous research (Polykretis et al., 2020; Schmidt et al., 2019), the erosion in Northeast China in this study exhibited a double-peak characteristic, namely, two erosion peaks were observed respectively in May and October (Fig. 4). This might be because in the south of the Northeast China, the long rainy season and the great intra-annual vegetation cover variation in broadleaf forests resulted in a unique double-peaked erosion feature at the beginning (May) and the end (October)of the rainy season with a low vegetation cover. As other studies has pointed out, when peak rainfall erosivity coincides with exposure of bare soils through, for example, bare fallow, forest harvesting, or land clearing, soil erosion risk is increased considerably (Panagos et al., 2012). In addition to erosive rainfall, periods of low vegetation cover are also critical for soil erosion, especially when the two coincide, which is the high-risk period for erosion. The determination of such a high-risk period varies for regions with different rainfall patterns and vegetation growth patterns, and requires targeted research conducted locally.

4.2. Impact of landform, climatic zone, and vegetation type on soil erosion

The spatial distribution of soil erosion is closely related to landform,

and our research shows that the erosion modulus increased with the increasing topography complexity, which was consistent with previous reports that steep mountainous areas usually have higher LS values (Gao et al., 2006), and the LS factor has an important effect on erosion modulus change (Campos et al., 2008; Souza et al., 2005).

The phenology of vegetation and seasonal soil erosion are closely related (Panagos et al., 2012; SAYGIN, 2021). The early-to-late order of turning green period of the four main vegetation types within the study area was: broadleaf forest > coniferous forest > crops > grassland (Meng, 2021). This corresponds to the order of the appearance of soil erosion peaks under different vegetation types. The earlier the turning green period, the earlier the vegetation coverage arose, indicating the earlier erosion decline (namely, reaching erosion peak earlier). Our findings regarding the erosion differences brought about by climatic zones in the north–south direction are consistent with previous studies (Ke and Zhang, 2021). However, in the east–west direction, there is an opposite pattern during the rainy season and the dry season. The pattern of east–west erosion changes in different climatic zones was related to the vegetation phenology pattern. During the rainy season, the erosion modulus of climatic zones decreased from east to west, which was consistent with the rainfall intensity decreasing from east to west in each climatic zone and the sequence of turning green periods of major vegetation type. During the non-rainy season, the erosion modulus in different climatic zones increasing from east to west was consistent with the early-to-late sequence of the turning yellowing periods of the main vegetation types (grassland > crop > broadleaf forest) (Meng, 2021). The earlier the vegetation entered the turning yellow period, the lower vegetation coverage, and the higher the erosion modulus.

4.3. *Recommendation proposed based on the controlling factors of soil erosion*

Identifying the main controlling factors of soil erosion will be of great significance for erosion control. For example, considering the strong influence of the LS factor, it is necessary to take erosion control measures in the areas with long slope length and steep slope such as converting sloping fields into terraces (Chen et al., 2016; Dorren and Rey, 2004). The contribution analysis of erosion factors showed that in different climatic zone subdivisions, the contributions of R factor and C factor varied with the rainy and dry seasons (Fig. 12). From north to south, the longer the rainy season was, the longer the time when C-factor played a dominant role. This indicated that good vegetation growth during the rainy season could effectively reduce the erosion damage, justifying the afforestation initiative (Porto et al., 2009; Zhou et al., 2006). The strong influence of R factor during the dry season suggested that even during non-rainy periods, the localized erosive rainfall could be an important driver of soil erosion, and thus it is particularly important to precisely control localized erosion according to meteorological conditions. Based on the driving results of erosional changes by R and C factors presented in Section 3.3, we believe that straw mulching when crop vegetation coverage is insufficient during February-June (Keesstra et al., 2019; Prosdocimi et al., 2016) and shrub or herbaceous vegetation planting in forest land (Jiang et al., 2019; Liu et al., 2020) will effectively mitigate the intensification of soil erosion. These measures are conducive to solving the problem of erosion increase before crop vegetation cover is sufficient and after the arrival of forest withering period.

5. Conclusion

This study assessed for the first time the monthly soil erosion risk in black soil regions of Northeast China by investigating dynamic rainfall and vegetation coverage based on RUSLE model. The result showed that the average annual soil erosion rate in Northeast China was 8.53 t•ha^{-1}•year^{-1}, and that the average monthly soil erosion rate was 0.78 t•ha^{-1}•month^{-1}. The high erosion risk period occurred in April-July and October, which coincided with the periods of low vegetation coverage and erosive rainfall. The areas at high erosion risk were mostly in western Inner Mongolia and southern Liaoning Province. Our results suggested that a monthly- resolution soil erosion assessment was necessary, and it would facilitate the identification of the periods and spatial units at the highest erosion risk that need attention.

The monthly erosion assessment can accurately reflect the natural variation pattern. Our data showed that LS, R, and C were the main factors controlling monthly soil erosion, making 30 %, 27.2 %, and 28.9 % of the contribution in the related periods, respectively. The R-factor and C-factor were the determinants affecting monthly soil erosion changes. With the vegetation growth period approaching, C-factor exhibited the increasingly strong influence and erosion resistance. Our findings will help local planners and decision makers to accurately understand the spatial and temporal variation of soil erosion and provide

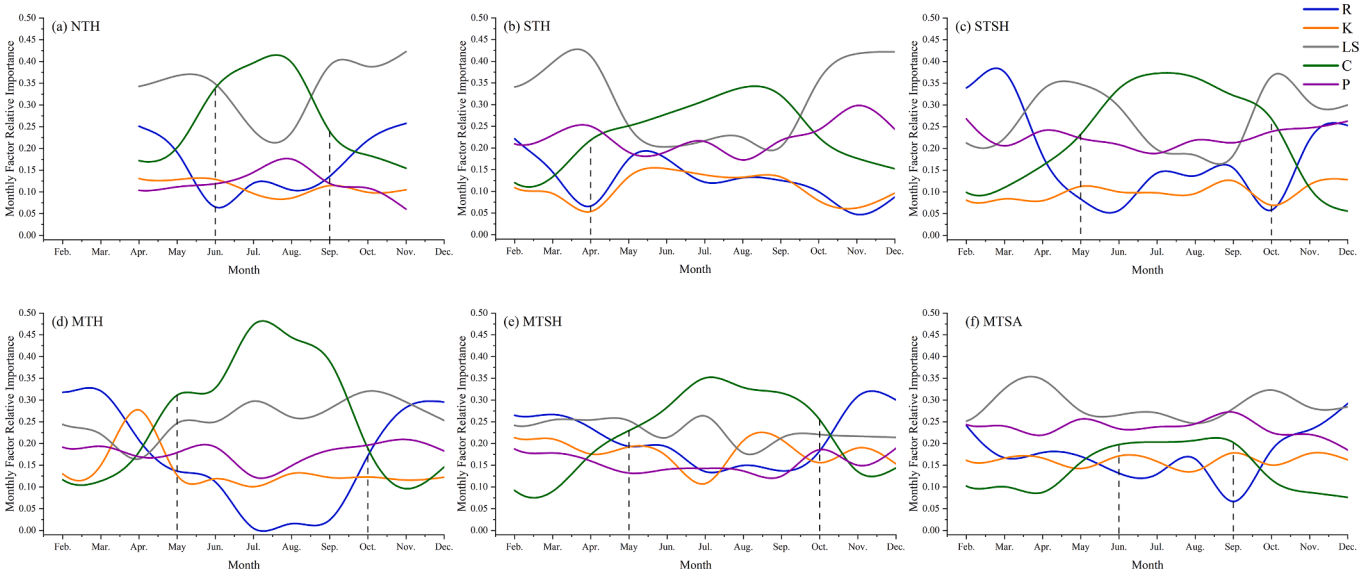

Fig. 12. Monthly contribution of erosion factors under different climate zones. (a) Northern temperate humid climate (NTH). (b) Southern temperate humid climate (STH). (c) Southern temperate sub-humid climate (STSH). (d) Middle temperate humid climate (MTH). (e) Middle temperate sub-humid climate (MTSH). (f) Middle temperate sub-arid climate (MTSH).

the theoretical basis for the formulation of potential soil conservation measures. It will be more beneficial to take some erosion control measures targeting at a specific area during the highest risk period.

CRediT authorship contribution statement

Yunfei Cao: Conceptualization, Data curation, Formal analysis, Methodology, Visualization, Writing – original draft. **Li Hua:** Conceptualization, Funding acquisition, Project administration, Resources, Writing – review & editing. **Qi Tang:** Data curation. **Lin Liu:** Data curation. **Chongfa Cai:** Funding acquisition, Project administration.

Declaration of Competing Interest

The authors declare the following financial interests/personal relationships which may be considered as potential competing interests: Li Hua reports financial support was provided by National Key Research and Development Program of China.

Data availability

The data that has been used is confidential.

Acknowledgements

Thank Soil Science Data Center, Institute of Soil Science, Chinese Academy of Sciences and other platforms for their data support. This research was supported by the National Key Research and Development Program of China (2021YFD1500703). I would like to express my sincere gratitude to my supervisor, Professor Li Hua, for her invaluable expertise in formulating research questions. I also want to thank Professor Feng Liu from the Nanjing Institute of Soil Science, Chinese Academy of Sciences, for providing the data support. In addition, I am grateful for the assistance provided by Mr. Yingjie Xu in conducting this study. Finally, I would like to thank the reviewers for their valuable suggestions to improve the manuscript.

References

Alexandridis, T.K., Sotiropoulou, A.M., Bilas, G., Karapetsas, N., Silleos, N.G., 2015. The effects of seasonality in estimating the C-factor of soil erosion studies. Land Degrad. Dev. 26 (6), 596–603.
Ang, B.W., 2004. Decomposition analysis for policymaking in energy: which is the preferred method? Energy Policy 32 (9), 1131–1139.
Ang, B.W., 2005. The LMDI approach to decomposition analysis: a practical guide. Energy Policy 33 (7), 867–871.
Ang, B.W., 2015. LMDI decomposition approach: A guide for implementation. Energy Policy 86, 233–238.
Baiamonte, G., Minacapilli, M., Novara, A., Gristina, L., 2019. Time scale effects and interactions of rainfall erosivity and cover management factors on vineyard soil loss erosion in the semi-arid area of southern Sicily. Water 11, 978.
Ballabio, C., Borrelli, P., Spinoni, J., Meusburger, K., Michaelides, S., Beguería, S., Klik, A., Petan, S., Janeček, M., Olsen, P., Aalto, J., Lakatos, M., Rymszewicz, A., Dumitrescu, A., Tadić, M.P., Diodato, N., Kostalova, J., Rousseva, S., Banasik, K., Alewell, C., Panagos, P., 2017. Mapping monthly rainfall erosivity in Europe. Sci. Total Environ. 579, 1298–1315.
Beskow, S., Mello, C.R., Norton, L.D., Curi, N., Viola, M.R., Avanzi, J.C., 2009. Soil erosion prediction in the Grande River Basin. Brazil using distributed modeling. Catena 79 (1), 49–59.
Blaikie, P., Brookfield, H., 2015. Land degradation and society. Routledge.
Borrelli, P., Märker, M., Panagos, P., Schütt, B., 2014. Modeling soil erosion and river sediment yield for an intermountain drainage basin of the Central Apennines. Italy. Catena 114, 45–58.
Campos, M.C.C., Marques Júnior, J., Martins Filho, M.V., Pereira, G.T., Souza, Z.M.d., Barbieri, D.M., 2008. Variação espacial da perda de solo por erosão em diferentes superfícies geomórficas. Ciência Rural 38 (9), 2485–2492.
Castro, R.M., dos Santos Alves, W., de Oliveira Marcionilio, S.M.L., de Moura, D.M.B., 2022. da Silva Oliveira DM. Soil losses related to land use and rainfall seasonality in a watershed in the Brazilian Cerrado. J. South Am. Earth Sci. 119, 104020.
Chen, D., Wei, W., Chen, L., Yun, Y., 2016. Progress of the ecosystem services and management of terraces. J. Mt. Sci 34, 374–384.
de Vente, J., Poesen, J., Govers, G., Boix-Fayos, C., 2009. The implications of data selection for regional erosion and sediment yield modelling. Earth Surf. Proc. Land. 34 (15), 1994–2007.
Delgado, D., Sadaoui, M., Ludwig, W., Méndez, W., 2022. Spatio-temporal assessment of rainfall erosivity in Ecuador based on RUSLE using satellite-based high frequency GPM-IMERG precipitation data. Catena 219, 106597.
Dorren, L., Rey, F., 2004. A review of the effect of terracing on erosion. In: Briefing Papers of the 2nd SCAPE Workshop. Citeseer, pp. 97–108.
Efthimiou, N., Psomiadis, E., Papanikolaou, I., Soulis, K.X., Borrelli, P., Panagos, P., 2022. A new high resolution object-oriented approach to define the spatiotemporal dynamics of the cover-management factor in soil erosion modelling. Catena 213, 106149.
Fan, H., Cai, Q., Chen, G., Cui, M., 2005. Comparative study of the soil erosion and control in the three major black soil regions in the world. J. Nat. Resour. 20, 387–393.
Fang, H., Fan, Z., 2020. Assessment of Soil Erosion at Multiple Spatial Scales Following Land Use Changes in 1980–2017 in the Black Soil Region, (NE) China. Int. J. Environ. Res. Public Health 17, 7378.
Fang, G., Yuan, T., Zhang, Y., Wen, X., Lin, R., 2019. Integrated study on soil erosion using RUSLE and GIS in Yangtze River Basin of Jiangsu Province (China). Arab. J. Geosci. 12, 1–13.
Feng, X.u., Suoyan, G., Zengxiang, Z., 2002. Soil erosion in China based on the 2000 national remote sensing survey. J. Geog. Sci. 12 (4), 435–442.
Fu, S., Liu, B., Zhou, G., Sun, Z., Zhu, X., 2015. Calculation tool of topographic factors. Science of Soil and Water Conservation 13, 105–110.
Gao, J., Liu, Y., Chen, Y., 2006. Land cover changes during agrarian restructuring in Northeast China. Appl. Geogr. 26 (3-4), 312–322.
Gelagay, H.S., Minale, A.S., 2016. Soil loss estimation using GIS and Remote sensing techniques: A case of Koga watershed, Northwestern Ethiopia. International Soil and Water Conservation Research 4 (2), 126–136.
He, Q., Dai, X., Chen, S., 2020. Assessing the effects of vegetation and precipitation on soil erosion in the Three-River Headwaters Region of the Qinghai-Tibet Plateau, China. J. Arid. Land 12 (5), 865–886.
Humphrey, O.S., Osano, O., Aura, C.M., Marriott, A.L., Dowell, S.M., Blake, W.H., Watts, M.J., 2022. Evaluating spatio-temporal soil erosion dynamics in the Winam Gulf catchment, Kenya for enhanced decision making in the land-lake interface. Sci. Total Environ. 815, 151975.
Jiang, M.-H., Lin, T.-C., Shaner, P.-J.L., Lyu, M.-K., Xu, C., Xie, J.-S., et al., 2019. Understory interception contributed to the convergence of surface runoff between a Chinese fir plantation and a secondary broadleaf forest. J. Hydrol. 574, 862–871.
Johannsen, L.L., Schmaltz, E.M., Mitrovits, O., Klik, A., Smoliner, W., Wang, S., Strauss, P., 2022. An update of the spatial and temporal variability of rainfall erosivity (R-factor) for the main agricultural production zones of Austria. Catena 215, 106305.
Ke, Q., Zhang, K., 2021. Patterns of runoff and erosion on bare slopes in different climate zones. Catena 198, 105069.
Keesstra, S., Rodrigo-Comino, J., Novara, A., Giménez-Morera, A., Pulido, M., Di Prima, S., et al., 2019. Straw mulch as a sustainable solution to decrease runoff and erosion in glyphosate-treated clementine plantations in Eastern Spain. An assessment using rainfall simulation experiments. Catena 174, 95–103.
Koirala, P., Thakuri, S., Joshi, S., Chauhan, R., 2019. Estimation of soil erosion in Nepal using a RUSLE modeling and geospatial tool. Geosciences 9, 147.
Le Roux, J., Morgenthal, T., Malherbe, J., Pretorius, D., Sumner, P., 2008. Water erosion prediction at a national scale for South Africa. Water SA 34, 305–314.
Lieskovský, J., Kenderessy, P., 2014. Modelling the effect of vegetation cover and different tillage practices on soil erosion in vineyards: a case study in Vráble (Slovakia) using WATEM/SEDEM. Land Degrad. Dev. 25 (3), 288–296.
Liu, Y.-F., Liu, Y., Shi, Z.-H., Lopez-Vicente, M., Wu, G.-L., 2020. Effectiveness of re-vegetated forest and grassland on soil erosion control in the semi-arid Loess Plateau. Catena 195, 104787.
Magesh, N., Chandrasekar, N., 2016. Assessment of soil erosion and sediment yield in the Tamiraparani sub-basin, South India, using an automated RUSLE-SY model. Environ. Earth Sci. 75, 1–17.
Meng, X., 2021. Temporal and Spatial Variation Characteristics of vegetation phenology and its response to climate factors in Northeast Asia. YanBian University.
Nations AOftU, 1998. World reference base for soil resources. Food & Agriculture Org.
Obalum, S.E., Buri, M.M., Nwite, J.C., Hermansah, Watanabe, Y., Igwe, C.A., Wakatsuki, T., 2012. Soil degradation-induced decline in productivity of sub-Saharan African soils: the prospects of looking downwards the lowlands with the Sawah ecotechnology. Appl. Environ. Soil Sci. 2012, 1–10.
Panagos, P., Karydas, C.G., Gitas, I.Z., Montanarella, L., 2012. Monthly soil erosion monitoring based on remotely sensed biophysical parameters: a case study in Strymonas river basin towards a functional pan-European service. Int. J. Digital Earth 5 (6), 461–487.
Panagos, P., Meusburger, K., Ballabio, C., Borrelli, P., Alewell, C., 2014. Soil erodibility in Europe: A high-resolution dataset based on LUCAS. Sci. Total Environ. 479, 189–200.
Phinzi, K., Ngetar, N.S., 2019. The assessment of water-borne erosion at catchment level using GIS-based RUSLE and remote sensing: A review. International Soil and Water Conservation Research 7 (1), 27–46.
Polykretis, C., Alexakis, D.D., Grillakis, M.G., Manoudakis, S., 2020. Assessment of intra-annual and inter-annual variabilities of soil erosion in Crete Island (Greece) by incorporating the Dynamic "Nature" of R and C-Factors in RUSLE modeling. Remote Sens. (Basel) 12, 2439.
Porto, P., Walling, D.E., Callegari, G., 2009. Investigating the effects of afforestation on soil erosion and sediment mobilisation in two small catchments in Southern Italy. Catena 79 (3), 181–188.
Prasannakumar, V., Vijith, H., Abinod, S., Geetha, N., 2012. Estimation of soil erosion risk within a small mountainous sub-watershed in Kerala, India, using Revised

Universal Soil Loss Equation (RUSLE) and geo-information technology. Geosci. Front. 3 (2), 209–215.
Prosdocimi, M., Jordán, A., Tarolli, P., Keesstra, S., Novara, A., 2016. The immediate effectiveness of barley straw mulch in reducing soil erodibility and surface runoff generation in Mediterranean vineyards. Science of the Total Environment 547, 323–330.
Renard, K.G., 1997. Predicting soil erosion by water: a guide to conservation planning with the Revised Universal Soil Loss Equation (RUSLE). United States Government Printing.
Renard, K., Foster, G., Weesies, G., Porter, J., 1991. RUSLE: revised universal soil loss equation. J. Soil Water Conserv. 46, 30–33.
Saygin, S., 2021. Effects of season and phenology-based changes on soil erodibility and other dynamic RUSLE factors for semi-arid winter wheat fields. Journal of Agricultural Sciences 27, 526–535.
Schmidt, S., Alewell, C., Meusburger, K., 2018. Mapping spatio-temporal dynamics of the cover and management factor (C-factor) for grasslands in Switzerland. Remote Sens. Environ. 211, 89–104.
Schmidt, S., Alewell, C., Meusburger, K., 2019. Monthly RUSLE soil erosion risk of Swiss grasslands. J. Maps 15 (2), 247–256.
Shi, D., Jiang, G., Peng, X., Jin, H., Jiang, N.a., 2021. Relationship between the periodicity of soil and water loss and erosion-sensitive periods based on temporal distributions of rainfall erosivity in the Three Gorges Reservoir Region, China. Catena 202, 105268.
Souza, Z.M.d., Martins Filho, M.V., Marques Júnior, J., Pereira, G.T., 2005. Variabilidade espacial de fatores de erosão em Latossolo Vermelho eutroférrico sob cultivo de cana-de-açúcar. Engenharia Agrícola 25 (1), 105–114.
Sujatha, E.R., Sridhar, V., 2018. Spatial Prediction of Erosion Risk of a small mountainous watershed using RUSLE: A case-study of the Palar sub-watershed in Kodaikanal South India. Water 10, 1608.
Sun, W., Shao, Q., Liu, J., Zhai, J., 2014. Assessing the effects of land use and topography on soil erosion on the Loess Plateau in China. Catena 121, 151–163.
Tiruwa, D.B., Khanal, B.R., Lamichhane, S., Acharya, B.S., 2021. Soil erosion estimation using Geographic Information System (GIS) and Revised Universal Soil Loss Equation (RUSLE) in the Siwalik Hills of Nawalparasi Nepal. Journal of Water and Climate Change 12, 1958–1974.
Wan, W., Liu, Z., Li, B., Fang, H., Wu, H., Yang, H., 2022. Evaluating soil erosion by introducing crop residue cover and anthropogenic disturbance intensity into cropland C-factor calculation: Novel estimations from a cropland-dominant region of Northeast China. Soil Tillage Res. 219, 105343.
Wang, S., Fang, H., He, J., 2021. Eeffects of variation in vegetation cover and rainfall on soil erosion in black soil region, northeastern China. Bull. Soil Water Conserv 41, 66–75.
Wang, B., Zhao, X., Wang, X., Zhang, Z., Yi, L., Hu, S., 2020. Spatial and temporal variability of soil erosion in the black soil region of Northeast China from 2000 to 2015. Environ. Monit. Assess. 192, 1–14.
Wei, C., Dong, X., Yu, D., Zhang, T.e., Zhao, W., Ma, Y., Su, B., 2022. Spatio-temporal variations of rainfall erosivity, correlation of climatic indices and influence on human activities in the Huaihe River Basin China. Catena 217, 106486.
Wen, D., Liang, W., 2001. Soil fertility quality and agricultural sustainable development in the black soil region of northeast China. Environ. Dev. Sustain. 3, 31–43.
William J, Arnold J. A system of erosion/sediment yield models. Reunion Internacional sobre Procesos de Erosion en Tierras de Altas Pendientes: Evaluacion y modelaje, Merida (Venezuela), 16-20 May 1993, 1993.
Williams, J., Renard, K., Dyke, P., 1983. EPIC: A new method for assessing erosion's effect on soil productivity. J. Soil Water Conserv. 38, 381–383.
Wischmeier, W.H., Smith, D.D., 1965. Predicting rainfall-erosion losses from cropland east of the. Rocky Mountains.
Xu, X.Z., Xu, Y., Chen, S.C., Xu, S.G., Zhang, H.W., 2010. Soil loss and conservation in the black soil region of Northeast China: a retrospective study. Environ Sci Policy 13 (8), 793–800.
Yan, Z., Bao-Yuan, L., Qing-Chun, Z., Yun, X., 2003. Effect of different vegetation types on soil erosion by water. J. Integr. Plant Biol. 45, 1204.
Yang, X., 2014. Deriving RUSLE cover factor from time-series fractional vegetation cover for hillslope erosion modelling in New South Wales. Soil Res. 52, 253–261.
Yang, X.M., Zhang, X.P., Deng, W., Fang, H.J., 2003. Black soil degradation by rainfall erosion in Jilin, China. Land Degradation & Development 14 (4), 409–420.
Yu, W., Ming-Yi, Y., Pu-Ling, L., 2010. Contribution partition of water and wind erosion on cultivated slopes in northeast black soil region of China. Journal of Nuclear Agricultural Sciences 24, 790.
Zhang, W., Fu, J., 2003. Rainfall erosivity estimation under different rainfall amount. Resources science 25, 35–41.
Zhang, W.-B., Xie, Y., Liu, B.-Y., 2002. Rainfall erosivity estimation using daily rainfall amounts. Scientia Geographica Sinica/Dili Kexue 22, 711–716.
Zhou, Z.C., Shangguan, Z.P., Zhao, D., 2006. Modeling vegetation coverage and soil erosion in the Loess Plateau Area of China. Ecol. Model. 198 (1-2), 263–268.